

# Liquid-Crystalline Perylene Diester Polymers with Tunable Charge-Carrier Mobility

Mathis-Andreas Muth, Miguel Carrasco-Orozco,\* and Mukundan Thelakkat\*

New classes of liquid-crystalline semiconductor polymers based on perylene diester benzimidazole and perylene diester imide mesogens are reported. Two highly soluble side-chain polymers, poly(perylenediester benzimidazole acrylate) (PPDB) and poly(perylenediester imide acrylate) (PPDI) are synthesized by nitroxide-mediated radical polymerization (NMRP). PPDB shows n-type semiconductor performance with electron mobilities of  $3.2 \times 10^{-4} \text{ cm}^2 \text{ V}^{-1} \text{ s}^{-1}$  obtained in a diode configuration by fitting the space-charge-limited currents (SCLC) according to the Mott–Gurney equation. Interestingly, PPDI performs preferentially as a p-type material with a hole mobility of  $1.5 \times 10^{-4} \text{ cm}^2 \text{ V}^{-1} \text{ s}^{-1}$ , which is attributed to the less electron-deficient perylene core of PPDI compared to PPDB. Optical properties are investigated by UV-vis and fluorescence spectroscopy. The extended  $\pi$ -conjugation system due to the benzimidazole unit of PPDB leads to a considerably broader absorption in the visible region compared to PPDI. HOMO and LUMO levels of the polymers are also determined by cyclic voltammetry; the resulting energy band-gaps are 1.86 eV for PPDB and 2.16 eV for PPDI. Thermal behavior and liquid crystallinity are studied by differential scanning calorimetry, polarized optical microscopy, and X-ray diffraction measurements. The results indicate liquid-crystalline order of the polymers over a broad temperature range. These thermal, electrical, and optical properties make the perylene side-chain polymers attractive materials for organic photovoltaics.

## 1. Introduction

The development of polymeric n-type semiconductors for electronic devices such as organic photovoltaic cells or organic field-effect transistors is still challenging and less extensively investigated, compared to the remarkable work done on p-type polymers recently.<sup>[1–3]</sup> Poor processability, insufficient electron mobilities, or lack of air-stability are current obstacles that have

to be overcome in designing novel n-type polymer materials.<sup>[4]</sup> The successful integration of a naphthalenedicarboxyimide based n-channel polymer into thin-film transistors, which leads to high electron mobilities under ambient conditions, was demonstrated recently.<sup>[5]</sup> In comparison, in donor–acceptor bulk-heterojunction solar cells, polymeric n-type materials used as electron acceptors show significantly lower performances than acceptors based on small molecules such as phenyl- $\text{C}_{61}$ -butyric acid methyl ester (PCBM).<sup>[6,7]</sup> Polymers however, usually show better film-forming properties than low molecular weight compounds.<sup>[8]</sup> This property is essential for solution processability, illustrating the need for n-type polymers. Perylene bisimides (PBI) are a relevant class of n-type semiconductors due to their relatively high electron affinity and strong visible-light absorption, combined with good photochemical and thermal stability.<sup>[9,10]</sup> Due to strong  $\pi$ – $\pi$  interaction of the perylene cores, electron mobilities of  $0.1$ – $1 \text{ cm}^2 \text{ V}^{-1} \text{ s}^{-1}$  for low molecular weight PBIs and  $1.2 \times 10^{-3} \text{ cm}^2 \text{ V}^{-1} \text{ s}^{-1}$  for a solution processable PBI side-chain homopolymer in organic field-effect transistors were reported.<sup>[11,12]</sup> It has been shown that, in terms of photoinduced charge generation, PBIs can be more effective electron acceptors than PCBM.<sup>[13]</sup> Due to comparatively poor device performance, this class of material has received limited attention in bulk heterojunction solar cells to date. The main issue is assumed to be an unfavorable blend morphology due to the tendency of PBI to form large crystals.<sup>[14]</sup> We reported recently on a series of highly soluble, low-molecular-weight discotic-liquid-crystalline (LC) PBI<sup>[15]</sup> and perylene diester benzimidazole (PDB) molecules.<sup>[16]</sup> The latter exhibit mesophases even at room temperature, combined with extended visible-light absorption compared to PBIs. The self-organization of discotic LC materials can be exploited in optoelectronic applications so that optimized morphology<sup>[17,18]</sup> and good charge-carrier transport properties along the  $\pi$ – $\pi$  stacking axis<sup>[19]</sup> can be combined. The concept of utilizing LC semiconducting polymers in organic photovoltaic cells,<sup>[20]</sup> as well as in organic light-emitting diodes (OLEDs)<sup>[21]</sup> and organic field-effect transistors (OFETs)<sup>[22]</sup> has been demonstrated successfully. In this context, to our knowledge, the polymerization of LC perylene benzimidazole moieties has not yet been reported.

M.-A. Muth, Prof. Dr. M. Thelakkat  
Applied Functional Polymers  
Department of Macromolecular Chemistry I  
University of Bayreuth  
Universitaetsstr. 30, 95440 Bayreuth, Germany  
E-mail: mukundan.thelakkat@uni-bayreuth.de  
Dr. M. Carrasco-Orozco  
Merck Chemicals Ltd  
Chilworth Technical Centre  
University Parkway  
Southampton SO16 7QD, UK  
E-mail: miguel.carrasco@merckgroup.com

DOI: 10.1002/adfm.201101694

Herein, we describe the synthesis of novel perylene side-chain homopolymers, based on LC perylene diester benzimidazole and perylene diester imide mesogens. Nitroxide-mediated radical polymerization (NMRP) was found to be a suitable method for the controlled synthesis of homopolymers and block copolymers based on acrylate monomers with pendant perylene moieties.<sup>[23–25]</sup> This radical polymerization method allows a metal-free polymerization of acrylate monomers giving narrow molecular-weight distributions. Additionally, a thorough characterization of LC phases by differential scanning calorimetry (DSC), polarized optical microscopy (POM), and X-ray diffraction measurements (XRD), and bulk electron-transport properties by the space-charge-limited current (SCLC) method are given.

## 2. Results and Discussion

### 2.1. Synthesis

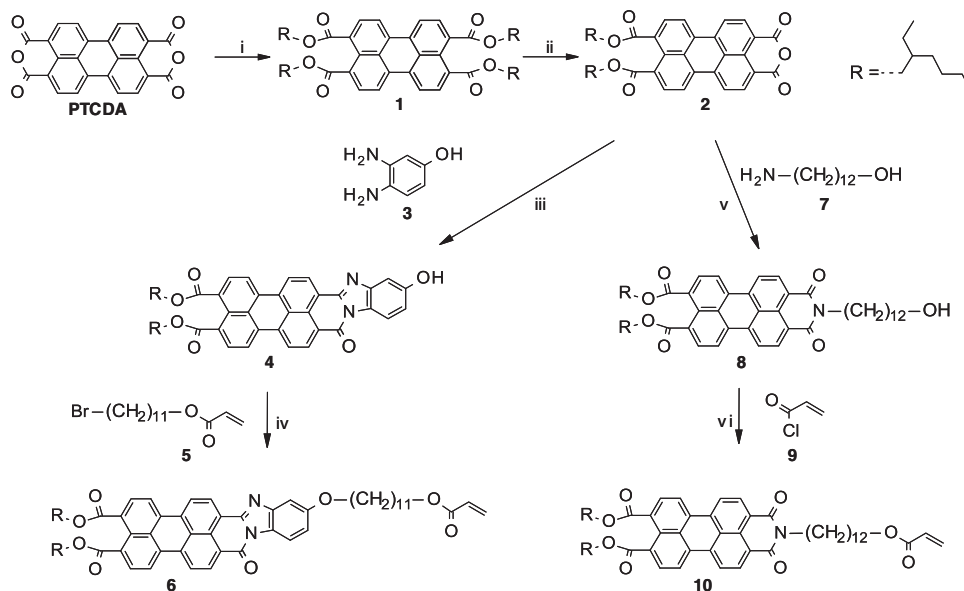
In this section, the synthesis of perylene acrylate monomers **6** and **10**, and their polymerization to the corresponding polymers PPDB and PPDI (see Scheme 2 for structures) via NMRP are described. The synthetic route to perylene acrylate monomers **6** and **10** is shown in Scheme 1. Perylene diester monoanhydride **2** was obtained from perylene-3,4,9,10-tetracarboxylic dianhydride (PTCDA) as the starting material according to a procedure described recently.<sup>[16]</sup> The branched aliphatic ethyl hexyl substituents linked to the ester groups give excellent solubility in various organic solvents. A benzimidazole unit was introduced to the perylene core by condensation reaction of **2** with 3,4-diaminophenol (**3**) to give perylene benzimidazole **4** carrying an OH group. This zinc acetate catalyzed reaction was

carried out under microwave irradiation with adequate yield (54%). Finally, to obtain monomer **6**, 11-bromoundecyl acrylate (**5**), bearing an acrylate moiety with alkyl spacer, was attached to **4** in a nucleophilic substitution under alkaline conditions. The acrylate unit of **5** serves as the polymerizable group and the alkyl chain provides sufficient flexibility to facilitate the polymerization in the presence of sterically hindering pendant perylene cores. The monomer **6** was obtained in 75% yield; the reaction conditions were similar to those in the perylene bisimide acrylate monomer synthesis described by Lindner and Thelakkat.<sup>[23]</sup>

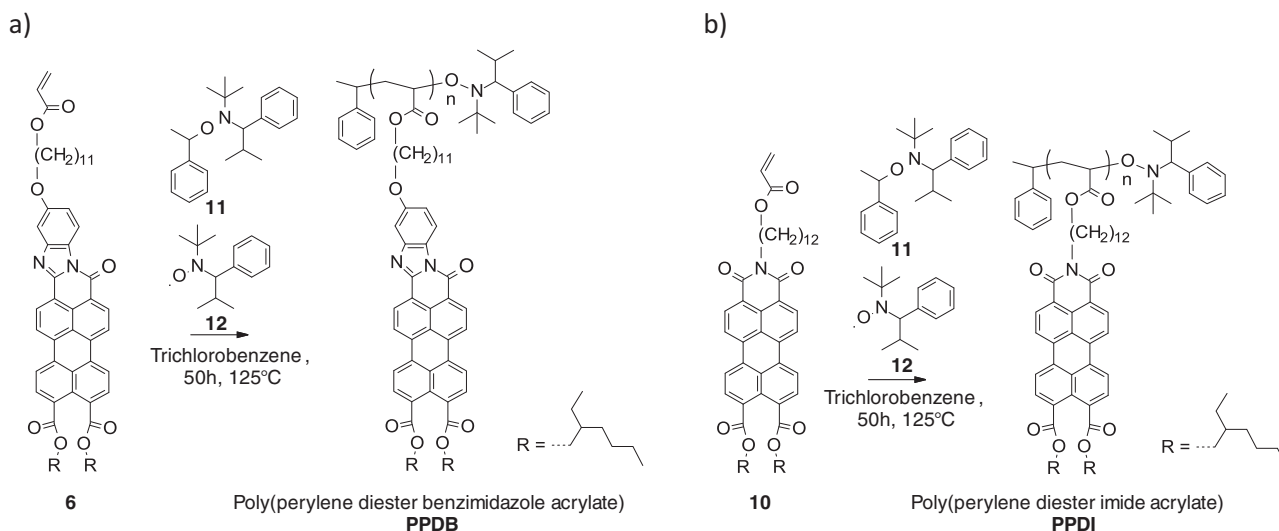
A second perylene diester acrylate monomer **10**, which includes an imide group instead of a benzimidazole unit, was synthesized to study the effect of the size of the conjugated  $\pi$ -system on optical, electronic and thermal properties. Monoanhydride diester **2** and the primary amine **7** were reacted to give the hydroxy-functionalized perylene diester imide **8**. The reaction was carried out in molten imidazole with an excess of **7** to give **8** in a high yield of 90%. The OH-group attached at the alkyl spacer served as functional group for esterification with acryloyl chloride (**9**). Finally, perylene diester imide acrylate **10** was obtained under basic conditions in a good yield of 68%.

A detailed description of the synthesis and purification of monomers, polymers and reactants **3**, **5**, and **7**, is given in the Experimental Section. All compounds were characterized by means of <sup>1</sup>H NMR and IR spectroscopy.

NMRP was utilized to homopolymerize monomers **6** and **10**. The reactants and the resultant perylene homopolymers PPDB and PPDI are depicted in Scheme 2. The ratio of monomer to 2,2,5-trimethyl-3-(1-phenylethoxy)-4-phenyl-3-azahexane (**11**), which served as unimolecular initiator, was [M]:[I] = 100:1. To shift the reaction equilibrium towards the dormant species, 0.1 equivalents of *N*-tert-butyl- $\alpha$ -isopropyl- $\alpha$ -phenylnitroxide (**12**) were added to the reaction mixture. This addition slowed



**Scheme 1.** Synthesis of perylene acrylate monomers **6** and **10**: i) 1. KOH/H<sub>2</sub>O, 0.5 h, 70 °C; 2. Aliquat 336, KI, 10 min, RT; 3. Br-R, 16 h, 100 °C. ii) *p*-toluenesulfonic acid monohydrate, toluene/*n*-dodecane, 5 h, 95 °C. iii) Zn(OAc)<sub>2</sub>/DMAc, 25 min, 160 °C, 300 W (microwave). iv) K<sub>2</sub>CO<sub>3</sub>, KI, DMAc, 17 h, 85 °C. v) Imidazole, Zn(OAc)<sub>2</sub>, 4 h, 160 °C. vi) Et<sub>3</sub>N/DCM, 24 h, 0 °C.



Scheme 2. Polymerization of a) 6 and b) 10 via NMRP.

the reaction rate and decreased the concentration of growing polymer radicals, which led to better control over the polymerization. The initiator **11** and free nitroxide **12** were synthesized according to a procedure described by Hawker and co-workers.<sup>[26]</sup> Only small amounts of solvent were used to prevent dilution of acrylate groups, so that the polymerization rate was not further decreased.

The reactions were quenched at a conversion of 35%, as determined by <sup>1</sup>H NMR, to prevent transfer reactions leading to increased molecular weight distributions.<sup>[27]</sup> The molecular weights of the polymers were identified by size-exclusion chromatography (SEC) in chlorobenzene, which was calibrated with polystyrene standards. The refractive-index-detector signals of the SEC traces of PPDB and PPDI are shown in Figure 1.

The number-average molecular weight ( $M_n$ ) and weight-average molecular weight ( $M_w$ ) of PPDB were found to be 9400 and 13300 g mol<sup>-1</sup>, respectively, with a polydispersity index (PDI) of 1.4. PPDI has a higher molecular weight of  $M_n = 20400$  g mol<sup>-1</sup> and  $M_w = 35300$  g mol<sup>-1</sup>, with a PDI of 1.7. Considering that a controlled radical-polymerization method was used, the molecular-weight distributions are rather broad. This result suggests that termination reactions took place, especially after long reaction times of 50 h. The higher molecular weights obtained for PPDI compared to PPDB are attributed to the

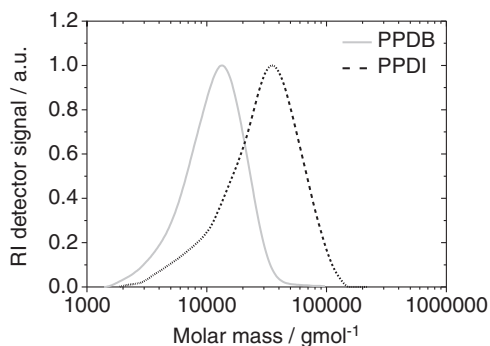


Figure 1. SEC traces (refractive-index detection) of PPDB and PPDI.

Table 1.  $M_n$ ,  $M_w$ , PDI, highest occupied molecular orbital (HOMO) and lowest unoccupied molecular orbital (LUMO) energy values and calculated band gap ( $E_g$ ) of PPDB and PPDI.

	$M_n$ [g mol <sup>-1</sup> ]	$M_w$ [g mol <sup>-1</sup> ]	PDI	HOMO [eV]	LUMO [eV]	$E_g$ [eV]
PPDB	9400	13300	1.4	-5.39	-3.53	1.86
PPDI	20400	35300	1.7	-5.68	-3.52	2.16

better solubility of PPDI in 1,2,4-trichlorobenzene. The high-molecular-weight PPDI is still soluble, whereas PPDB becomes insoluble after reaching an average molecular weight ( $M_n$ ) of above 10000 g mol<sup>-1</sup>, which decreases the further polymerization rate significantly. SEC data are summarized in Table 1.

## 2.2. Polymer Characterization

### 2.2.1. Thermotropic Properties

The thermotropic behavior of the two polymers was studied by using DSC, POM, and XRD. The DSC traces shown in Figure 2a and b were recorded at a scanning rate of 10 K min<sup>-1</sup>. Phase-transition temperatures and the corresponding enthalpies  $\Delta H$  are summarized in Table 2. The first heating cycles were ignored to rule out an influence of the thermal history of the samples. For PPDB a glass transition ( $T_g$ ) at 151 °C and a reversible phase transition to an isotropic state at 312 °C were found. The comparatively small enthalpy of 3.8 J g<sup>-1</sup> suggests a phase transition from an LC mesophase to the isotropic melt. The corresponding crystallization peak upon cooling was detected at 279 °C. The existence of a LC phase was confirmed by POM, which was equipped with a temperature-controlled hot stage. Upon cooling from the isotropic state with a cooling rate of 3 K min<sup>-1</sup>, birefringent textures under crossed polarizers for PPDB were observed, which are shown in Figure 2c. The image was obtained at a temperature of 300 °C. The sample was a viscous liquid, which indicates an LC rather than a crystalline

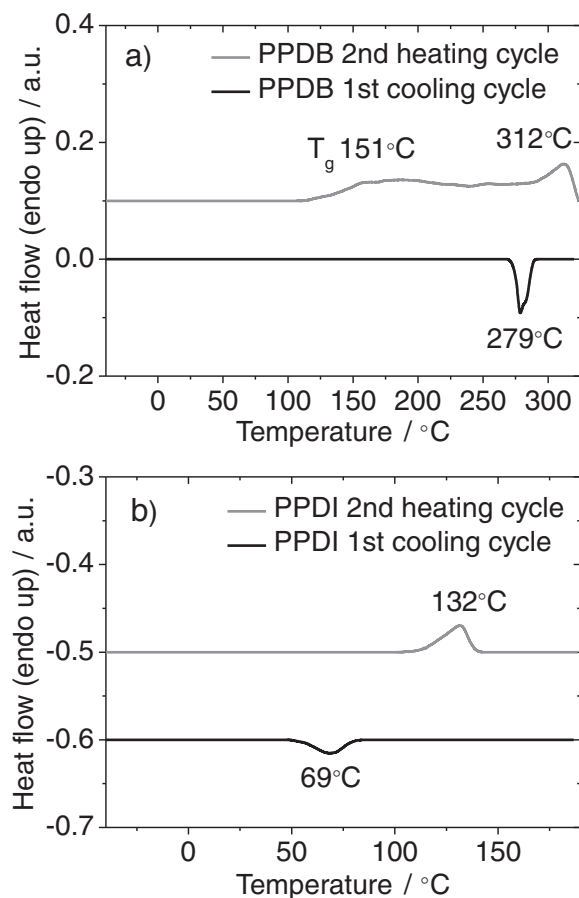


**Figure 2.** DSC thermogram (scan rate  $10 \text{ K min}^{-1}$ ) for a) PPDB and b) PPDI showing the second heating and the first cooling cycle. Peak values for the phase transitions are given. Optical microscopy images (polarizers crossed) of the LC mesophases of c) PPDB at  $300^\circ\text{C}$  and d) PPDI at  $110^\circ\text{C}$ . The textures were obtained upon cooling the sample from the isotropic melt and annealing at the respective temperature.

**Table 2.** Phase behavior of PPDB and PPDI obtained from DSC measurements. g: glassy, LC: liquid crystalline, I: isotropic.

	Phase transitions and corresponding enthalpies $\Delta H$	
	2 <sup>nd</sup> heating cycle ( $T/^\circ\text{C}$ ; $\Delta H/\text{J g}^{-1}$ )	1 <sup>st</sup> cooling cycle ( $T/^\circ\text{C}$ ; $\Delta H/\text{J g}^{-1}$ )
PPDB	g (151) $\rightarrow$ LC (312; 3.8) $\rightarrow$ I	I (279; 3.7) $\rightarrow$ LC
PPDI	LC (132; 2.8) $\rightarrow$ I	I (69; 1.6) $\rightarrow$ LC

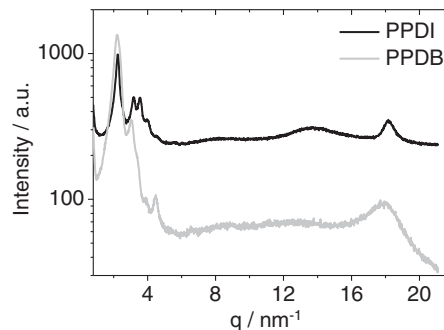


**Figure 3.** X-ray diffraction pattern of PPDI recorded at room temperature after annealing at  $140^\circ\text{C}$  and PPDB recorded at  $250^\circ\text{C}$ .

phase. The temperature difference observed for the phase transition between POM ( $300^\circ\text{C}$ ) and DSC ( $279^\circ\text{C}$ ) is due to the supercooling effect caused by a faster cooling rate in the DSC measurement. Similar observations were made for PPDI, where the melting point was identified at  $132^\circ\text{C}$  by DSC and POM. In the same way, the small transition enthalpy ( $2.8 \text{ J g}^{-1}$ ) in DSC and birefringent textures under crossed polarizers in POM (Figure 2d) indicate that PPDI also exhibits an LC mesophase. Figure 2d was obtained after annealing PPDI at  $110^\circ\text{C}$  for 5 h. The absence of other phase transitions in the DSC traces implies that PPDI is still in the liquid-crystalline state at room temperature, however the viscosity of the compounds increases with decreasing temperature and crystallization of the materials might be thus kinetically hindered.

To further verify the thermotropic liquid-crystalline character of both polymers, X-ray scattering experiments were carried out. The instrument was equipped with a Guinier camera and a hot stage. The XRD patterns of PPDB and PPDI are shown in Figure 3. As reported recently,<sup>[16]</sup> for LC perylene derivatives a columnar hexagonal ordering of the disclike mesogens is often observed. According to the X-ray diffractogram (Figure 3), the packing behavior of the perylene side-chain polymers PPDB and PPDI could not be identified as columnar hexagonal. Here, the Bragg reflections in the low  $q$  regime are indicative of a 2D columnar rectangular or columnar oblique ordering.<sup>[28]</sup> To clarify the particular structure of the mesophases, additional temperature-dependent small-angle X-ray scattering (SAXS) experiments will be carried out at ESRF Grenoble. In the wide-angle regime of the PPDB diffractogram a comparatively broad reflection at a  $q$  value of  $17.89 \text{ nm}^{-1}$  corresponds to a short-range repeat distance of  $3.51 \text{ \AA}$ . This distance can be attributed to the  $\pi$ - $\pi$  stacking distance of perylene cores of adjacent polymer side-chains. For PPDI a clearly sharper reflection at  $q = 18.21 \text{ nm}^{-1}$  depicts a  $\pi$ - $\pi$  stacking distance of  $3.45 \text{ \AA}$ . The more defined and sharper reflection and the closer packing distance of PPDI compared to PPDB demonstrate a slightly better organization and more regular packing of the perylene cores. It is important to mention that PPDB, in contrast to PPDI, was not heated above the melting temperature before measurement due to temperature limitations of our X-ray instrument. Therefore the preconditions for self-organization were not similar for the two polymers. More detailed temperature-dependent wide-angle X-ray scattering (WAXS) experiments are currently

being performed. An amorphous halo and the absence of further reflections at high  $q$  values verify the liquidlike character of the alkyl chains. In conclusion, PPDB and PPDI are liquid crystalline; the latter even at room temperature.

### 2.2.2. Optical and Electronic Properties

The two homopolymers PPDB and PPDI were investigated in terms of their absorption behavior in solution and in solid state, their HOMO and LUMO levels, and their charge-carrier mobilities. The UV-vis absorption spectra of PPDB and PPDI in chlorobenzene solution and in thin films are shown in Figure 4a. Characteristic vibronic bands for perylene diester imide PPDI, similar to those of PBI-based homopolymers,<sup>[29]</sup> are found. The three vibronic transitions in solution at 510, 479, and 450 nm are hypsochromically shifted by 20 nm compared to in the PBI homopolymer. The fluorescence maximum of PPDI measured in film with an excitation wavelength of 525 nm is at 573 nm (Figure 4b). The presence of a benzimidazole unit in PPDB extends the absorption considerably, up to 670 nm in solution and 680 nm in film, with an absorption maximum at 530 nm. Thus the absorption edge of PPDB is red-shifted by almost 100 nm compared to in PPDI. Neither vibronic fine structure in the absorption spectra nor fluorescence could be observed for PPDB. A spectral broadening for both polymers in thin films, compared to the solution spectra is observed, which indicates a change in aggregation in the solid state.

Cyclic voltammetry was carried out to estimate HOMO/LUMO levels and study electrochemical stability of the compounds. To determine LUMO energy values, each measurement was calibrated with the ferrocene–ferrocenium couple (Fc/Fc<sup>+</sup>) taking 4.8 eV as ferrocene's HOMO level.<sup>[30]</sup> The cyclic voltammograms (Figure 5) show two reversible reduction peaks for both polymers, characteristic for the perylene unit. The first reduction peaks occurring at –1.27 V for PPDB and –1.28 V for PPDI result in almost identical LUMO energy levels of –3.53 and –3.52 eV, respectively. Up to five cycles were recorded and no changes in the redox peaks were observed, which indicates electrochemical stability and reversibility. HOMO values were estimated from the optical band-gap and the LUMO levels. The optical band-gap, obtained from the absorption edges of absorption spectra in chlorobenzene solution (see Figure 4a), was found to be 1.86 eV for PPDB and 2.16 eV for PPDI. The resulting HOMO and LUMO energy levels and band-gaps are summarized in Table 1.

UV-vis absorption measurements and cyclic voltammetry both demonstrate the effect of the benzimidazole unit in PPDB on optical and electronic properties. The  $\pi$ -conjugation system of the perylene core is enlarged compared to PPDI, due to the fused benzimidazole moiety in PPDB, which leads to an increase in delocalized  $\pi$ -electrons. Therefore, less energy is needed to excite an electron from the HOMO to the LUMO in PPDB, which explains the bathochromic shift in absorption spectra and the lowered band-gap. Strong light harvesting in the visible range and favorable energy levels are important

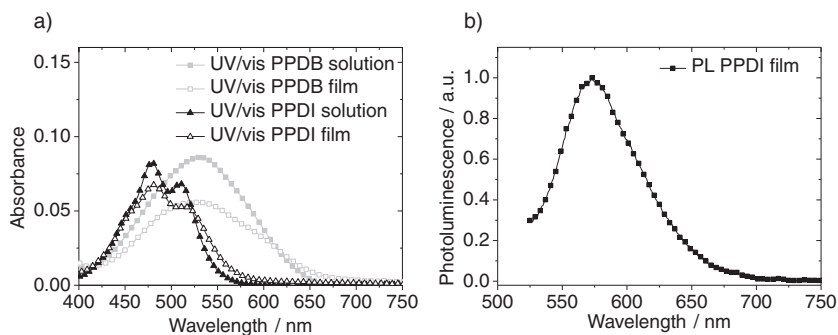


**Figure 4.** a) UV–vis absorption spectra of PPDB and PPDI measured in chlorobenzene solution and in thin films and b) photoluminescence spectra of PPDI thin film ( $\lambda_{\text{ex}} = 525$  nm).

prerequisites for use in organic electronic devices such as photovoltaic cells. In addition, the charge-carrier mobility is a crucial feature.

To determine the bulk charge-carrier mobilities of both polymers, current–voltage  $I$ – $V$  characteristics of each material sandwiched between two electrodes were measured and the space-charge-limited currents (SCLC) were fitted according to the Mott–Gurney equation,<sup>[31]</sup>

$$J = \frac{9}{8} \cdot \epsilon_r \cdot \epsilon_0 \cdot \mu_0 \cdot e^{0.89 \cdot \gamma \cdot \sqrt{E}} \cdot \frac{V^2}{L^3} \quad (1)$$

where  $J$  is the current density,  $\epsilon_r$  is the dielectric constant of the polymer (assumed to be 3 in our calculations<sup>[32]</sup>),  $\epsilon_0$  is the permittivity of free space,  $\mu_0$  is the zero-field charge-carrier mobility,  $\gamma$  is the field-activation parameter,  $E$  is the electric field,  $L$  is the thickness of the polymer layer, and  $V$  is the voltage drop across the device.

This method estimates the material's charge-carrier mobility in the bulk. In comparison, OFET measurements only measure the charge transport within a very narrow sheet at the interface with the gate insulator.<sup>[32–34]</sup> Charge-carrier densities in OFET devices are orders of magnitude higher than in organic solar cells or organic light-emitting diodes. Since charge-carrier mobilities depend on charge-carrier densities, the mobility values obtained from OFETs do not necessarily describe the bulk carrier transport at low carrier densities like those in

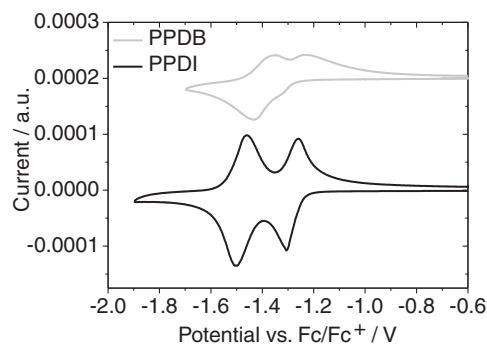


**Figure 5.** Cyclic voltammograms of PPDB and PPDI showing the first and second reduction peaks. The measurements were conducted in acetonitrile with respect to Fc/Fc<sup>+</sup> at a scan rate of 50 mV s<sup>–1</sup>.

organic photovoltaic devices. Furthermore, initial testing of the two polymers under investigation in OFET devices show poor performance, which we attribute to potential unfavorable alignment of the active material in the channel of the transistor; this does not seem problematic for SCLC devices, since architecture and underlying layers are different from those of OFET devices. Two different types of SCLC devices were fabricated to determine both electron and hole mobilities of the perylene polymers. Electron-only devices based on PPDB and PPDI comprise a poly(3,4-ethylenedioxythiophene):poly(styrenesulfonate) (PEDOT:PSS) covered indium–tin oxide (ITO) bottom contact and a calcium top electrode capped with aluminum. The device architecture is depicted in Figure 6a. Calcium has a work function of 2.9 eV and serves as an ohmic contact for electron injection into the LUMO of PPDB and PPDI (ca. 3.5 eV). Concurrently, the bottom contact does not hinder electrons from leaving the device. Hole-only devices (Figure 6b) were fabricated correspondingly with an ITO/PEDOT:PSS bottom contact, but with a gold top electrode instead of calcium. The low work function of gold (5.1 eV) provides a large mismatch with the LUMO of PPDB and PPDI, which prevents electron injection and therefore holes injected from the bottom electrode are

the dominant charge carriers in these devices. The polymer layer thicknesses of the single-carrier devices were varied from 300–650 nm.  $I$ – $V$  characteristics of the devices were recorded at up to 6 V at room temperature in an inert gas atmosphere. The experimental data and the corresponding fits according to Equation 1 are shown in Figure 6c–f. For calculation, voltages were corrected for a built-in potential of 2.2 eV from the difference in work function of calcium (ca. 2.9 eV) and ITO/PEDOT:PSS (ca. 5.1 eV) for electron-only devices.<sup>[35]</sup> At high voltages the current is space-charge-limited only, assuming ohmic contacts to the injecting electrode. In this regime, the current density approximately scales with  $J \sim V^2$ , so the charge-carrier mobility at zero-field  $\mu_0$  and the field-activation parameter  $\gamma$  can be determined by fitting the curve according to Equation 1. The values obtained for  $\mu_0$  and  $\gamma$  for the best fits are summarized in Table 3. Inserting these values into Equation 2<sup>[34]</sup>

$$\mu = \mu_0 \cdot e^{\gamma \cdot \sqrt{E}} \quad (2)$$

yields the charge-carrier mobilities  $\mu$  depending on the electric field within the device. Table 3 shows the charge-carrier mobilities calculated for the maximum electric field.

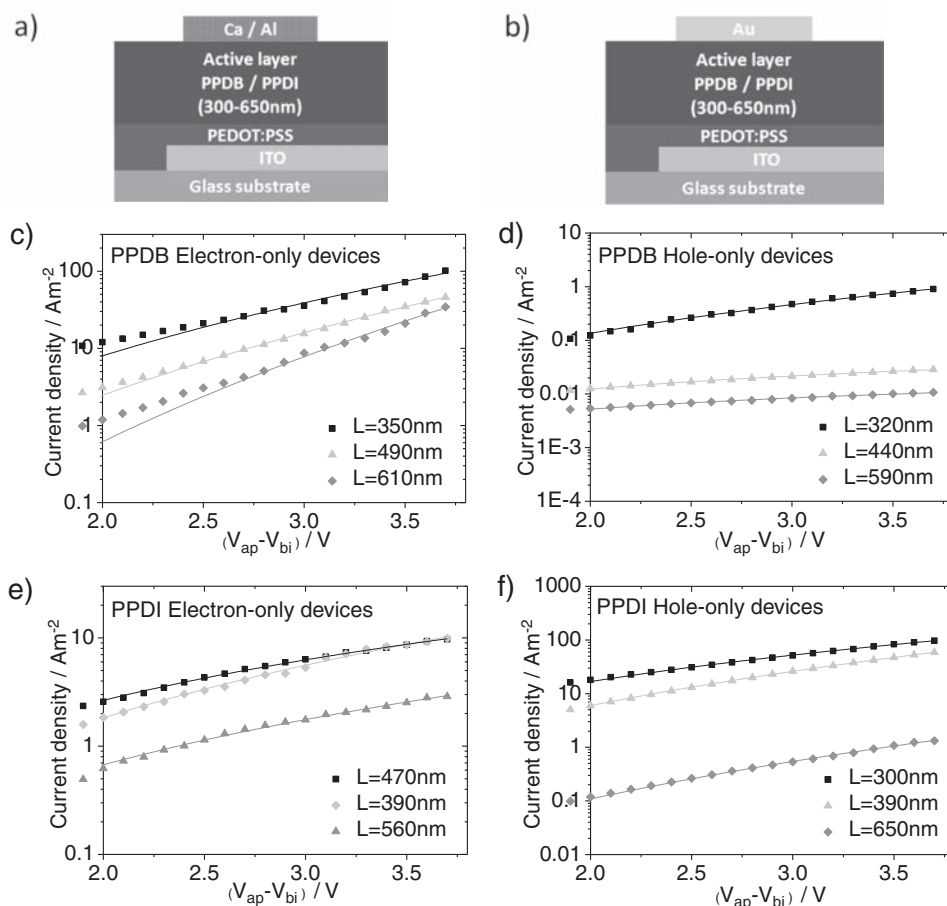


**Figure 6.** Scheme of a) an electron-only device with a calcium top electrode, capped with aluminum and b) a hole-only device with gold top electrode, current density  $J$  vs. voltage  $V$  plots (data points) and fits according to Equation 1 (straight lines) at room temperature for c) PPDB electron-only devices, d) PPDB hole-only devices, e) PPDI electron-only devices, and f) PPDI hole-only devices with varied layer thicknesses  $L$ . The voltage applied ( $V_{ap}$ ) was corrected for a built-in potential ( $V_{bi}$ ) of 2.2 eV for electron-only devices resulting from the differences in work function of calcium and ITO/PEDOT:PSS.  $V_{bi}$  in hole-only devices was estimated to be 0 eV.

**Table 3.** SCLC charge carrier mobilities and associated field activation parameters for PPDB and PPDI.

	Electron mobility			Hole mobility		
	$\mu_{0e}$ [cm <sup>2</sup> V <sup>-1</sup> s <sup>-1</sup> ]	$\gamma$ [m <sup>0.5</sup> V <sup>-0.5</sup> ]	$\mu_e$ [cm <sup>2</sup> V <sup>-1</sup> s <sup>-1</sup> ]	$\mu_{0h}$ [cm <sup>2</sup> V <sup>-1</sup> s <sup>-1</sup> ]	$\gamma$ [m <sup>0.5</sup> V <sup>-0.5</sup> ]	$\mu_h$ [cm <sup>2</sup> V <sup>-1</sup> s <sup>-1</sup> ]
PPDB	$2.2 \cdot 10^{-7}$	$2.6 \cdot 10^{-3}$	$3.2 \cdot 10^{-4}$	$6.0 \cdot 10^{-8}$	$8.2 \cdot 10^{-4}$	$1.0 \cdot 10^{-6}$
PPDI	$2.3 \cdot 10^{-6}$	$6.8 \cdot 10^{-4}$	$1.9 \cdot 10^{-5}$	$1.6 \cdot 10^{-6}$	$1.5 \cdot 10^{-3}$	$1.5 \cdot 10^{-4}$

$\mu_0$  and  $\gamma$  values were obtained by fitting the  $J$ - $V$  curves of the single carrier devices according to equation 1.  $\mu$  was determined from equation 2 and the maximum electric field in the device.

Using this method, the electron mobility  $\mu_e$  was found to be  $3.2 \times 10^{-4}$  cm<sup>2</sup> V<sup>-1</sup> s<sup>-1</sup> for PPDB and the hole mobility  $\mu_h$  was determined to be  $1.0 \times 10^{-6}$  cm<sup>2</sup> V<sup>-1</sup> s<sup>-1</sup>. The hole mobility is two orders of magnitude smaller than the electron mobility, thus this polymer can be considered an n-type semiconductor. PPDI has an electron mobility of  $1.9 \times 10^{-5}$  cm<sup>2</sup> V<sup>-1</sup> s<sup>-1</sup> and a hole mobility of  $1.5 \times 10^{-4}$  cm<sup>2</sup> V<sup>-1</sup> s<sup>-1</sup>. The results from the SCLC measurements are summarized in Table 3. Interestingly, the hole mobility of PPDI is nearly one order of magnitude higher than its electron mobility. As a result, we assign PPDI to a new class of p-type materials. In contrast to perylene bisimides, which are well-known electron acceptors because of their two electron-withdrawing imide groups,<sup>[36]</sup> the perylene core of PPDI only contains one imide group. This imide content results in a less electron-deficient character and therefore a more donor-type behavior. In comparison, the benzimidazole unit of PPDB provides enough electron deficiency in the heterocyclic aromatic system to enhance the electron-accepting properties of this material. We therefore demonstrate here that the electronic character of perylene side-chain polymers can be tuned by modifying the aromatic perylene core.

### 3. Conclusion

In summary, two novel liquid-crystalline perylene diester side chain homopolymers were synthesized via nitroxide-mediated radical polymerization. We have demonstrated that changing the heterocyclic  $\pi$ -system permits access to materials with different electronic character. PPDB has n-type semiconducting properties with an electron mobility of  $3.2 \times 10^{-4}$  cm<sup>2</sup> V<sup>-1</sup> s<sup>-1</sup>, whereas PPDI shows p-type behavior with a hole mobility of  $1.5 \times 10^{-4}$  cm<sup>2</sup> V<sup>-1</sup> s<sup>-1</sup>, as determined from SCLC measurements. Altering the aromatic system of the perylene core not only affects the electrical properties of the investigated polymers; the absorption of PPDB in the visible range is notably broadened up to 670 nm compared to PPDI (580 nm), which is due to extension of  $\pi$ -conjugation of the perylene core by the benzimidazole unit of PPDB. The optical band-gaps as determined by the absorption edge of UV-vis measurements and cyclic voltammetry were 1.86 eV for PPDB and 2.16 eV for PPDI, with similar LUMO energy levels of -3.53 and -3.52 eV, respectively. Furthermore, the ethyl hexyl substituents attached to the ester groups of the perylene core give excellent solubility in common organic solvents. These findings qualify the two polymers as potential materials for application in optoelectronic devices, which will be the subject of future investigations. Thermotropic

behavior of PPDB and PPDI was studied by using polarized optical microscopy, differential scanning calorimetry, and X-ray diffraction. Both polymers exhibit liquid-crystalline mesophases over a broad temperature range.

### 4. Experimental Section

**Instrumentation:** <sup>1</sup>H NMR spectra were recorded using a Bruker AC 300 spectrometer (300 MHz) at 25 °C with deuterated chloroform as solvent and tetramethylsilane as an internal standard. Chemical shifts are reported in ppm, abbreviations used for splitting patterns are *s* = singlet, *d* = doublet, *t* = triplet, *q* = quartet, *m* = multiplet. FTIR data were recorded with a Perkin Elmer Spectrum 100 (FTIR) in the range 400–4000 cm<sup>-1</sup>. Molecular-weight determinations were carried out in chlorobenzene solution at 60 °C on an Agilent 1100 series GPC using two Polymer Laboratories mixed B columns in series. The system was calibrated against narrow weight PL polystyrene calibration standards. DSC measurements were performed on a TA Q1000 under nitrogen with a heating and cooling rate of 10 K min<sup>-1</sup>. Phase transitions were also examined using a POM Nikon Diaphot 300 with a Mettler FP 90 temperature controlled hot stage. XRD measurements were performed on a Huber Guinier Diffraktometer 6000 equipped with a Huber quartz monochromator 611 with Cu K $\alpha_1$ : 1.54051 Å. UV-vis spectra of solutions in chlorobenzene with a concentration of 10<sup>-5</sup> mol L<sup>-1</sup> and thin films spin-cast on quartz glass were recorded on a Hitachi 3000 spectrophotometer. Photoluminescence spectra were acquired on a Shimadzu RF 5301 PC spectrofluorophotometer upon excitation at 525 nm. Cyclic voltammetry (CV) was recorded on a Princeton Applied Research VersaSTAT 4 Potentiostat/Galvanostat using platinum electrodes at a scan rate of 50 mV s<sup>-1</sup> and an Ag/Ag<sup>+</sup> (0.10 M AgNO<sub>3</sub> in acetonitrile) reference electrode at 25 °C in an anhydrous and nitrogen-saturated solution of 0.1 M tetrabutylammonium tetrafluoroborate (Bu<sub>4</sub>NBF<sub>4</sub>) in acetonitrile. In these conditions, the oxidation potential of ferrocene was 0.10 V versus Ag/Ag<sup>+</sup>, whereas the oxidation potential of ferrocene was 0.41 V versus saturated calomel electrode (SCE). The LUMO energy levels were determined from the reduction peak taking into account the SCE level at -4.7 eV. Film thicknesses were determined on an Alphastep 500 surface profilometer.

**Chemicals:** The starting materials, perylenetetracarboxylic acid dianhydride (PTCDA), 3-(bromomethyl)heptane, Aliquat 336, *p*-toluenesulfonic acid monohydrate, zinc acetate, 11-bromoundecanol, sodium cyanide, Raney Ni, acryloyl chloride, and solvents were purchased from Aldrich, Fluka, or Acros and used without any further purification. Solvents used for precipitation and column chromatography were distilled prior to use. Dimethyl acetate (DMAc; anhydrous with crown cap, 99.5%), dimethyl sulfoxide (DMSO; anhydrous with crown cap, 99.5%) and 1,2,4 trichlorobenzene (anhydrous with crown cap, 99.0%) were purchased from Aldrich. PEDOT:PSS (Clevios P VP Al 4083) was purchased from Heraeus.

The preparation of **1** and **2** was described recently by Wicklein et al.<sup>[16]</sup> **5** was prepared according to Lang et al.<sup>[27]</sup> The initiator **11** and the free nitroxide **12** were synthesized according to published procedures.<sup>[26]</sup>

**Synthesis of 3,4-Diaminophenol (3):** 4-amino-3-nitrophenol (6.5 mmol, 1.00 g) and palladium on charcoal (0.10 g, 10%) were added to

methanol (55 mL) under an inert gas atmosphere. The reaction flask was flushed with hydrogen twice before stirring the reaction mixture for 3.5 h at room temperature under a hydrogen atmosphere. The solution was filtered through Celite under an argon atmosphere. After the solvent was evaporated under reduced pressure, the product was obtained in quantitative yield as a brownish white solid, which was unstable in air and used immediately upon preparation.

**Synthesis of Bis(2-ethylhexyl)-perylene-3,4-(4-hydroxy-1,2-benzimidazole)-9,10-dicarboxylate (4):** **2** (2.4 mmol, 1.50 g), zinc acetate (3.5 mmol, 0.65 g), and **3** (4.7 mmol, 0.59 g) were dissolved in dry DMAc (50 mL) in a microwave pressure tube. The condensation reaction was carried out under microwave irradiation conditions for 30 min at 150 °C and 100 W. The violet crude product was precipitated in methanol (300 mL) and filtered. The residue was washed with water (2 × 30 mL) and methanol (3 × 30 mL) and dried overnight at 60 °C in vacuo. The crude product was purified using column chromatography (silica flash gel, eluent chloroform:methanol 9:1 v/v). Yield: 0.90 g (53%) as a violet solid. <sup>1</sup>H NMR (300 MHz, CDCl<sub>3</sub>, 298 K, δ): 8.45–8.38 (m, 1H, H<sub>A1</sub>), 8.32–8.09 (m, 5H, H<sub>A1</sub>), 8.03–7.91 (m, 2H, H<sub>A1</sub>), 7.64–7.57 (m, 1H, H<sub>A1</sub>), 6.62–6.59 (m, 1H, OH), 6.42–6.28 (m, 2H, H<sub>A1</sub>), 4.44–4.26 (m, 4H, OCH<sub>2</sub>), 1.96–1.80 (m, 2H, OCH<sub>2</sub>CH), 1.72–1.17 (m, 16H, CH<sub>2</sub>), 1.14–0.94 (m, 12H, CH<sub>3</sub>); IR (ATR): ν = 3360 (b), 2960 (m), 2930 (m), 2860 (m), 1691 (s), 1593 (s), 1445 (m), 1362 (s), 1260 (s), 1171 (s), 804 (s), 745 (s) cm<sup>-1</sup>.

**Synthesis of Bis(2-ethylhexyl)-perylene-3,4-(4-undecyloxyacrylic acid-1,2-benzimidazole)-9,10-dicarboxylate (6):** **4** (0.7 mmol, 0.51 g), **5** (1.4 mmol, 0.43 g), potassium carbonate (1.4 mmol, 0.19 g), and potassium iodide (0.14 mmol, 0.02 g) were dissolved in dry DMAc (20 mL) and stirred for 24 h at 85 °C under an argon atmosphere. The crude product was precipitated in a mixture of methanol and water (MeOH:H<sub>2</sub>O 3:1 v/v, 150 mL), filtered and washed (2 × MeOH:H<sub>2</sub>O 3:1 v/v, 30 mL). The residue was dried overnight at 60 °C in vacuo. The crude product was purified using column chromatography (silica flash gel, eluent chloroform:acetone 95:5 v/v). Yield: 0.59 g (88%) as a violet solid. <sup>1</sup>H NMR (300 MHz, CDCl<sub>3</sub>, 298 K, δ): 8.74–8.62 (m, 2H, H<sub>A1</sub>), 8.48–8.31 (m, 5H, H<sub>A1</sub>), 8.10–8.01 (m, 2H, H<sub>A1</sub>), 7.30 (m, 1H, H<sub>A1</sub>), 7.07–7.00 (m, 1H, H<sub>A1</sub>), 6.42 (dd, *2*J = 17.3 Hz, *3*J = 1.6 Hz, 1H, acryl-CH<sub>2</sub>), 6.14 (dd, *2*J = 17.3 Hz, *3*J = 10.4 Hz, 1H, acryl-CH), 5.83 (dd, *2*J = 10.4 Hz, *3*J = 1.5 Hz, 1H, acryl-CH<sub>2</sub>), 4.37–4.25 (m, 4H, OCH<sub>2</sub>), 4.18 (t, *J* = 6.8 Hz, 2H, acryl-OCH<sub>2</sub>), 4.07 (m, 2H, benzimidazole-OCH<sub>2</sub>), 1.94–1.77 (m, 4H, OCH<sub>2</sub>CH, benzimidazole-OCH<sub>2</sub>CH<sub>2</sub>), 1.75–1.63 (m, 2H, acryl-OCH<sub>2</sub>CH<sub>2</sub>), 1.60–1.24 (m, 30H, CH<sub>2</sub>), 1.06–0.88 (m, 12H, CH<sub>3</sub>); IR (ATR): ν = 2926 (s), 2856 (m), 1712 (s), 1688 (s), 1592 (m), 1466 (m), 1268 (s), 1171 (s), 1062 (m), 804 (s), 742 (m) cm<sup>-1</sup>.

**Synthesis of 12-Hydroxydodecanenitrile:** The synthesis was adapted from the work of Jaeger et al.<sup>[37]</sup> A mixture of 11-bromoundecanol (20.0 mmol, 5.00 g), sodium cyanide (38.9 mmol, 1.91 g), and DMSO (75 mL) was stirred for 24 h at 90 °C. Then the reaction mixture was added to water (150 mL) and extracted four times with DCM (4 × 100 mL). The combined extracts were washed six times with water, dried over sodium sulfate, and the solvent was removed on the rotary evaporator to give 3.85 g (98%) product. <sup>1</sup>H NMR (300 MHz, CDCl<sub>3</sub>, 298 K, δ): 3.65 (q, *J* = 6.3 Hz, 2H, CH<sub>2</sub>O), 2.35 (t, *J* = 7.1 Hz, 2H, CH<sub>2</sub>CN), 1.74–1.52 (m, 5H, CH<sub>2</sub>CH<sub>2</sub>CN, OH), 1.51–1.40 (m, 2H, CH<sub>2</sub>CH<sub>2</sub>O), 1.38–1.24 (br s, 12H, (CH<sub>2</sub>)<sub>6</sub>); IR (ATR): ν = 3383 (m), 2919 (s), 2851 (s), 2248 (m), 1470 (s), 1335 (m), 1053 (s), 1013 (m), 722 (s) cm<sup>-1</sup>.

**Synthesis of 12-Aminododecan-1-ol (7):** The synthesis was adapted from the work of Jaeger et al.<sup>[37]</sup> A mixture of 12-hydroxydodecanenitrile (19.3 mmol, 3.80 g), Raney Ni (38.9 mmol, 5.00 g), ethanol (80 mL, 95%), and concentrated ammonium hydroxide (50 mL, 25%) was stirred under a hydrogen atmosphere for 20 h at room temperature. Then the reaction mixture was filtered through a pad of Celite, which was washed with ethanol (50 mL, 95%). The combined filtrates were concentrated on the rotary evaporator to give 3.6 g (95%) **7**. <sup>1</sup>H NMR (300 MHz, CDCl<sub>3</sub>, 298 K, δ): 3.65 (t, *J* = 6.5 Hz, 2H, CH<sub>2</sub>O), 2.71 (br s, 2H, NH<sub>2</sub>), 1.64–1.52 (m, 2H, CH<sub>2</sub>CH<sub>2</sub>NH<sub>2</sub>), 1.51–1.41 (m, 2H, CH<sub>2</sub>CH<sub>2</sub>O), 1.29 (br s, 19H, OH, (CH<sub>2</sub>)<sub>9</sub>); IR (ATR): ν = 3329 (m), 3286 (m), 2917 (s), 2849 (s), 1614 (m), 1470 (s), 1372 (m), 1065 (s), 1044 (m), 999 (m), 855 (w), 828 (w), 719 (s) cm<sup>-1</sup>.

**Synthesis of N-(dodecyl-1-ol)-bis(2-ethylhexyl)-perylene-3,4,9,10-tetracarboxyl-monoimide (8):** A mixture of **2** (6.0 mmol, 3.86 g), imidazole (350 mmol, 24 g) and **7** (9.1 mmol, 1.84 g) was stirred for 2 h at 130 °C. After cooling to room temperature the mixture was dissolved in tetrahydrofuran (THF; 1 mL), precipitated in water (200 mL), and filtered. The residue was washed with water (2 × 30 mL) and dried overnight at 60 °C in vacuo. The crude product was purified using column chromatography (silica flash gel, eluent chloroform:acetone 20:1 v/v). Yield: 4.47 g (90%) as an orange-red solid. <sup>1</sup>H NMR (300 MHz, CDCl<sub>3</sub>, 298 K, δ): 8.63 (d, *J* = 8.0 Hz, 2H, H<sub>A1</sub>), 8.47 (dd, *2*J = 8.2 Hz, *3*J = 4.6 Hz, 4H, H<sub>A1</sub>), 8.10 (d, *J* = 7.9 Hz, 2H, H<sub>A1</sub>), 4.38–4.27 (m, 4H, OCH<sub>2</sub>), 4.25–4.16 (m, 2H, OCH<sub>2</sub>), 3.70–3.62 (m, 2H, NCH<sub>2</sub>), 1.87–1.72 (m, 4H, OCH<sub>2</sub>CH, OCH<sub>2</sub>), 1.61–1.22 (m, 35H, CH<sub>2</sub>, OH), 1.04–0.88 (m, 12H, CH<sub>3</sub>); IR (ATR): ν = 3505 (w), 2924 (s), 2854 (m), 1695 (s), 1652 (s), 1593 (s), 1511 (m), 1356 (m), 1294 (s), 1261 (s), 1171 (s), 1076 (s), 956 (m), 846 (m), 806 (m), 745 (s) cm<sup>-1</sup>.

**Synthesis of N-(Dodecylacrylic acid)-bis(2-ethylhexyl)-perylene-3,4,9,10-tetracarboxyl-monoimide (10):** **8** (4.3 mmol, 3.5 g) was dissolved in dry THF (120 mL) under an argon atmosphere and potassium carbonate (8.6 mmol, 1.8 g) was added. Acryloyl chloride (19.3 mmol, 1.74 g) was added dropwise at 0 °C and the reaction mixture was stirred for 20 h at 60 °C. The mixture was poured into water (100 mL) and the crude product was extracted with chloroform (3 × 100 mL). The combined extracts were washed with water (3 × 100 mL), dried over sodium sulfate, and the solvent was removed on the rotary evaporator. The crude product was purified using column chromatography (silica flash gel, eluent chloroform:acetone 20:1 v/v). Yield: 2.50 g (67%) as an orange-red solid. <sup>1</sup>H NMR (300 MHz, CDCl<sub>3</sub>, 298 K, δ): 8.62 (d, *J* = 8.0 Hz, 2H, H<sub>A1</sub>), 8.45 (dd, *2*J = 8.2 Hz, *3*J = 3.3 Hz, 4H, H<sub>A1</sub>), 8.09 (d, *J* = 7.9 Hz, 2H, H<sub>A1</sub>), 6.41 (dd, *2*J = 17.3 Hz, *3*J = 1.6 Hz, 1H, acryl-CH<sub>2</sub>), 6.13 (dd, *2*J = 17.3 Hz, *3*J = 10.4 Hz, 1H, acryl-CH), 5.82 (dd, *2*J = 10.4 Hz, *3*J = 1.5 Hz, 1H, acryl-CH<sub>2</sub>), 4.38–4.26 (m, 4H, OCH<sub>2</sub>), 4.25–4.10 (m, 4H, acryl-OCH<sub>2</sub>, NCH<sub>2</sub>), 1.89–1.74 (m, 4H, OCH<sub>2</sub>CH, acryl-OCH<sub>2</sub>CH<sub>2</sub>), 1.74–1.60 (m, 2H, NCH<sub>2</sub>CH<sub>2</sub>), 1.58–1.21 (m, 32H, CH<sub>2</sub>), 1.05–0.86 (m, 12H, CH<sub>3</sub>); IR (ATR): ν = 2957 (m), 2925 (s), 2855 (s), 1723 (s), 1695 (s), 1652 (s), 1593 (s), 1511 (m), 1356 (s), 1294 (s), 1260 (s), 1171 (s), 1076 (s), 984 (m), 961 (m), 847 (m), 806 (s), 745 (s) cm<sup>-1</sup>.

**Synthesis of Poly(perylene diester benzimidazole acrylate) (PPDB):** A mixture of **6** (1.0 mmol, 740 mg), **11** (0.01 mmol, 3.2 mg), **12** (0.001 mmol, 0.22 mg), and 1,2,4-trichlorobenzene (1250 μL) was degassed using three freeze/thaw cycles, sealed under argon and heated for 50 h at 125 °C. The reaction mixture was cooled, dissolved in chloroform (4 mL), precipitated in acetone (250 mL), and filtered. The residue was dried and further purified by Soxhlet extraction with methyl ethyl ketone. Yield: 0.26 g (35%) as a violet powder. GPC: *M*<sub>n</sub> = 9400 g mol<sup>-1</sup>, *M*<sub>w</sub> = 13300 g mol<sup>-1</sup>, PDI = 1.4.

**Synthesis of Poly(perylene diester imide acrylate) (PPDI):** A mixture of **10** (1.7 mmol, 1500 mg), **11** (0.017 mmol, 5.3 mg), **12** (0.0017 mmol, 0.37 mg), and 1,2,4-trichlorobenzene (915 μL) was degassed using three freeze/thaw cycles, sealed under argon, and heated for 50 h at 125 °C. The reaction mixture was cooled, dissolved in chloroform (3 mL), precipitated in methanol (250 mL), and filtered. The residue was dried and further purified by Soxhlet extraction with acetone. Yield: 0.48 g (32%) as an orange powder. GPC: *M*<sub>n</sub> = 20400 g mol<sup>-1</sup>, *M*<sub>w</sub> = 35300 g mol<sup>-1</sup>, PDI = 1.7.

**SCLC Devices:** SCLC electron-only devices were fabricated using the following structure: glass/ITO/PEDOT:PSS/polymer/Ca/Al. SCLC hole-only devices were fabricated using the following structure: glass/ITO/PEDOT:PSS/polymer/Au. Commercial ITO-coated glass substrates with a sheet resistance of 13 Ohms per sq (Lumtec) were cleaned using the following sequence in an ultrasonic bath: water, acetone, and 2-propanol. Each ITO substrate was patterned using photolithography techniques. After ozone treatment of the substrates for 5 min, PEDOT:PSS was spin-coated onto the ITO surface and dried at 130 °C for 30 min. All following steps were carried out under a nitrogen atmosphere with water and oxygen levels ≤0.1 ppm. After cooling the substrate, the polymer layer was blade-coated from chloroform solutions. The substrates were then put in a thermal evaporation chamber to evaporate the top electrode (30 nm Ca/100 nm Al for electron-only devices, 80 nm Au for hole-only devices) under high vacuum (1 × 10<sup>-6</sup> mbar) through a shadow mask

(active area 4 mm<sup>2</sup>). The current–voltage characteristics of the devices were measured using a Keithley 2420 (I–V) Digital SourceMeter at 25 °C.

## Acknowledgements

Financial support from Merck Chemicals Ltd. and EU-India project “largecells” is kindly acknowledged.

Please note: This article was amended on December 6, 2011 to correct a mistake in Table 3 of the version that was first published online.

Received: July 22, 2011

Published online: October 21, 2011

- [1] L.-L. Chua, J. Zaumseil, J.-F. Chang, E. C. W. Ou, P. K. H. Ho, H. Sirringhaus, R. H. Friend, *Nature* **2005**, 434, 194.
- [2] K. M. Coakley, M. D. McGehee, *Chem. Mater.* **2004**, 16, 4533.
- [3] Y. Liang, Z. Xu, J. Xia, S. T. Tsai, Y. Wu, G. Li, C. Ray, L. Yu, *Adv. Mater.* **2010**, 22, E135.
- [4] Z. Chen, Y. Zheng, H. Yan, A. Facchetti, *J. Am. Chem. Soc.* **2008**, 131, 8.
- [5] H. Yan, Z. Chen, Y. Zheng, C. Newman, J. R. Quinn, F. Dotz, M. Kastler, A. Facchetti, *Nature* **2009**, 457, 679.
- [6] X. Zhan, Z. a. Tan, B. Domercq, Z. An, X. Zhang, S. Barlow, Y. Li, D. Zhu, B. Kippelen, S. R. Marder, *J. Am. Chem. Soc.* **2007**, 129, 7246.
- [7] M. Koppe, H. J. Egelhaaf, G. Dennler, M. C. Scharber, C. J. Brabec, P. Schilinsky, C. N. Hoth, *Adv. Funct. Mater.* **2010**, 20, 338.
- [8] J. Kang, N. Shin, D. Y. Jang, V. M. Prabhu, D. Y. Yoon, *J. Am. Chem. Soc.* **2008**, 130, 12273.
- [9] B. Jancy, S. K. Asha, *J. Phys. Chem. B* **2006**, 110, 20937.
- [10] Y. Avlasevich, C. Li, K. Mullen, *J. Mater. Chem.* **2010**, 20, 3814.
- [11] B. A. Jones, A. Facchetti, M. R. Wasielewski, T. J. Marks, *J. Am. Chem. Soc.* **2007**, 129, 15259.
- [12] S. Hüttner, M. Sommer, M. Thelakkat, *Appl. Phys. Lett.* **2008**, 92, 093302.
- [13] S. Shoaee, Z. An, X. Zhang, S. Barlow, S. R. Marder, W. Duffy, M. Heeney, I. McCulloch, J. R. Durrant, *Chem. Commun.* **2009**, 5445.
- [14] J. J. Dittmer, E. A. Marseglia, R. H. Friend, *Adv. Mater.* **2000**, 12, 1270.
- [15] A. Wicklein, A. Lang, M. Muth, M. Thelakkat, *J. Am. Chem. Soc.* **2009**, 131, 14442.
- [16] A. Wicklein, M.-A. Muth, M. Thelakkat, *J. Mater. Chem.* **2010**, 20, 8646.
- [17] L. Schmidt-Mende, A. Fechtenkotter, K. Mullen, E. Moons, R. H. Friend, J. D. MacKenzie, *Science* **2001**, 293, 1119.
- [18] J. L. Li, M. Kastler, W. Pisula, J. W. F. Robertson, D. Wasserfallen, A. C. Grimsdale, J. S. Wu, K. Müllen, *Adv. Funct. Mater.* **2007**, 17, 2528.
- [19] S. Sergeev, W. Pisula, Y. H. Geerts, *Chem. Soc. Rev.* **2007**, 36, 1902.
- [20] M. Carrasco-Orozco, W. C. Tsoi, M. O'Neill, M. P. Aldred, P. Vlachos, S. M. Kelly, *Adv. Mater.* **2006**, 18, 1754.
- [21] P. A. Levermore, R. Jin, X. Wang, J. C. de Mello, D. D. C. Bradley, *Adv. Funct. Mater.* **2009**, 19, 950.
- [22] I. McCulloch, M. Heeney, C. Bailey, K. Genevicius, I. MacDonald, M. Shkunov, D. Sparrowe, S. Tierney, R. Wagner, W. Zhang, M. L. Chabinyc, R. J. Kline, M. D. McGehee, M. F. Toney, *Nat. Mater.* **2006**, 5, 328.
- [23] S. M. Lindner, M. Thelakkat, *Macromolecules* **2004**, 37, 8832.
- [24] A. S. Lang, F. R. Kogler, M. Sommer, U. Wiesner, M. Thelakkat, *Macromol. Rapid Commun.* **2009**, 30, 1243.
- [25] Q. Zhang, A. Cirpan, T. P. Russell, T. Emrick, *Macromolecules* **2009**, 42, 1079.
- [26] D. Benoit, V. Chablinski, R. Braslau, C. J. Hawker, *J. Am. Chem. Soc.* **1999**, 121, 3904.
- [27] A. S. Lang, A. Neubig, M. Sommer, M. Thelakkat, *Macromolecules* **2010**, 43, 7001.
- [28] S. Laschat, A. Baro, N. Steinke, F. Giesselmann, C. Hägele, G. Scalia, R. Judele, E. Kapatsina, S. Sauer, A. Schreivogel, M. Tosoni, *Angew. Chem. Int. Ed.* **2007**, 46, 4832.
- [29] M. Sommer, S. Hüttner, S. Wunder, M. Thelakkat, *Adv. Mater.* **2008**, 20, 2523.
- [30] J. Pommerehne, H. Vestweber, W. Guss, R. F. Mahrt, H. Bässler, M. Porsch, J. Daub, *Adv. Mater.* **1995**, 7, 551.
- [31] P. W. M. Blom, C. Tanase, D. M. d. Leeuw, R. Coehoorn, *Appl. Phys. Lett.* **2005**, 86, 092105.
- [32] C. Goh, R. J. Kline, M. D. McGehee, E. N. Kadnikova, J. M. J. Frechet, *Appl. Phys. Lett.* **2005**, 86, 122110.
- [33] R. Steyrlleuthner, M. Schubert, F. Jaiser, J. C. Blakesley, Z. Chen, A. Facchetti, D. Neher, *Adv. Mater.* **2010**, 22, 2799.
- [34] Z. An, J. Yu, B. Domercq, S. C. Jones, S. Barlow, B. Kippelen, S. R. Marder, *J. Mater. Chem.* **2009**, 19, 6688.
- [35] V. D. Mihailetchi, J. K. J. van Duren, P. W. M. Blom, J. C. Hummelen, R. A. J. Janssen, J. M. Kroon, M. T. Rispens, W. J. H. Verhees, M. M. Wienk, *Adv. Funct. Mater.* **2003**, 13, 43.
- [36] S. Alibert-Fouet, I. Seguy, J.-F. Bobo, P. Destruel, H. Bock, *Chem. Eur. J.* **2007**, 13, 1746.
- [37] D. A. Jaeger, R. Jose, A. Mendoza, R. P. Apkarian, *Colloids Surf. A* **2007**, 302, 186.